JWMM

Advanced Survey Techniques for Port Infrastructure Assessment: A Collision Investigation Case Study

Nguyen Hoang Anh Thu[1,2,3], Ly Dang Khoa[1,2,3], Tran Phuc Minh Khoi[1,2,3], Nguyen Le Thanh Phuoc[1,2,3], and Nguyen Danh Thao[1,2]

[1]*Ho Chi Minh City University of Technology (HCMUT), Vietnam*

[2]*Vietnam National University, Ho Chi Minh City, Vietnam*

[3]*Portcoast Consultant Corporation, Ho Chi Minh City, Vietnam*

DOI: https://doi.org/10.14796/JWMM.S544

ABSTRACT

This paper presents a case study demonstrating the effective integration of advanced technologies for a comprehensive current conditions survey following a collision accident at the Interflour port's waterfront jetty in Phu My town, Ba Ria, Vung Tau province, Vietnam. To reconstruct the accident and assess the port's future operability, a combination of 3D laser scanning, unmanned aerial vehicle (UAV) aerial photography, bathymetric surveying by unmanned surface vehicles (USVs), and side-scan sonar for marine obstacle detection were conducted. 3D laser scanning provided high-precision data (up to 1.0 mm accuracy) for modeling and simulations of above-water structures. UAVs enabled detailed inspection of the vast jetty area. USVs generated accurate bathymetric maps, while side-scan sonar detected underwater obstacles. Data from all sources was integrated into a Geographic Information System (GIS) platform for streamlined management and analysis. The paper aims to highlight the value of technological solutions in accident investigations. Integrating these methods facilitates highly accurate data collection and visualization, even in challenging environments. The results have implications for improving survey accuracy and efficiency, supporting the assessment and restoration of critical infrastructure following accidents.

1 INTRODUCTION

In the construction industry, bathymetric surveys, topographic surveys, marine obstacles detection by side-scan sonar, and sub-bottom profiling provide accurate measurements and project efficiency (Gillins et al. 2022). Unlike traditional topographic surveying methods using total stations and Real-Time Kinematic (RTK) point collection, which yield individual elevation

Thu, N.H.A., L.D. Khoa, T.P.M. Khoi, N.L.T. Phuoc, and N.D. Thao. 2025. "Advanced Survey Techniques for Port Infrastructure Assessment: A Collision Investigation Case Study." *Journal of Water Management Modeling* 33: S544. https://doi.org/10.14796/JWMM.S544 www.chijournal.org ISSN: 2292-6062

points, modern surveying techniques employing advanced laser scanners, and UAVs generate highly precise point cloud datasets (Thao et al. 2024). Topographic surveys use total stations, Global Positioning System/Global Navigation Satellite System (GPS/GNSS) receivers, and Light Detection and Ranging (LiDAR) equipped drones to develop comprehensive maps that show site contours, elevations, and characteristics (Gillins et al. 2022). Bathymetric surveys use single-beam and multi-beam echosounders to assess the depth and features of the underwater terrain. Marine obstacle detection by side-scan sonar helps detect obstacles or structures below the water surface (Healy et al. 2015). Sub-bottom profiling employs reflection signals to identify and characterize geological layers for seabed evaluation in the survey area (NOAA Ocean Exploration 2023; NOAA Ocean Exploration 2014). To ensure safe passage and efficient dredging operations, this data is essential for constructing and operating ports, harbours, and other infrastructure projects in general. Bathymetric surveys offer engineers insights into the distribution of sediment and underwater uncertainties, which they can use to design solid structures that have enough bearing capacity to resist (Khoi et al. 2024).

However, comprehensive data capturing for post-incident assessment, even in complex environments, is still a challenging solution (Ehlers 2011). This paper outlines the field survey work process implemented following a vessel collision incident. The survey aimed to capture comprehensive data for post-incident assessment, including terrestrial elevation data on the affected land areas, water depth measurements, identification of obstacles such as collapsed structures, and mapping of the affected seabed surface both before and after the removal of obstacles. The use of modern surveying technologies plays a vital role in acquiring more precise and detailed data compared to traditional methods. This case study draws upon the experience and lessons learned from the Interflour Cai Mep Port project in southern Vietnam (detailed in Figure 1). Notably, this port experienced two separate vessel collisions with the wharf structure within a short timeframe (February and July 2023, as shown in Figures 2 and 3). The outlined procedure has the potential to minimize the time required for recovery and restoration efforts in similar future incidents.

Figure 1 Location of project in Vung Tau, Thi Vai channel.

Figure 2 Port situation after the 1st incident in February 2023.

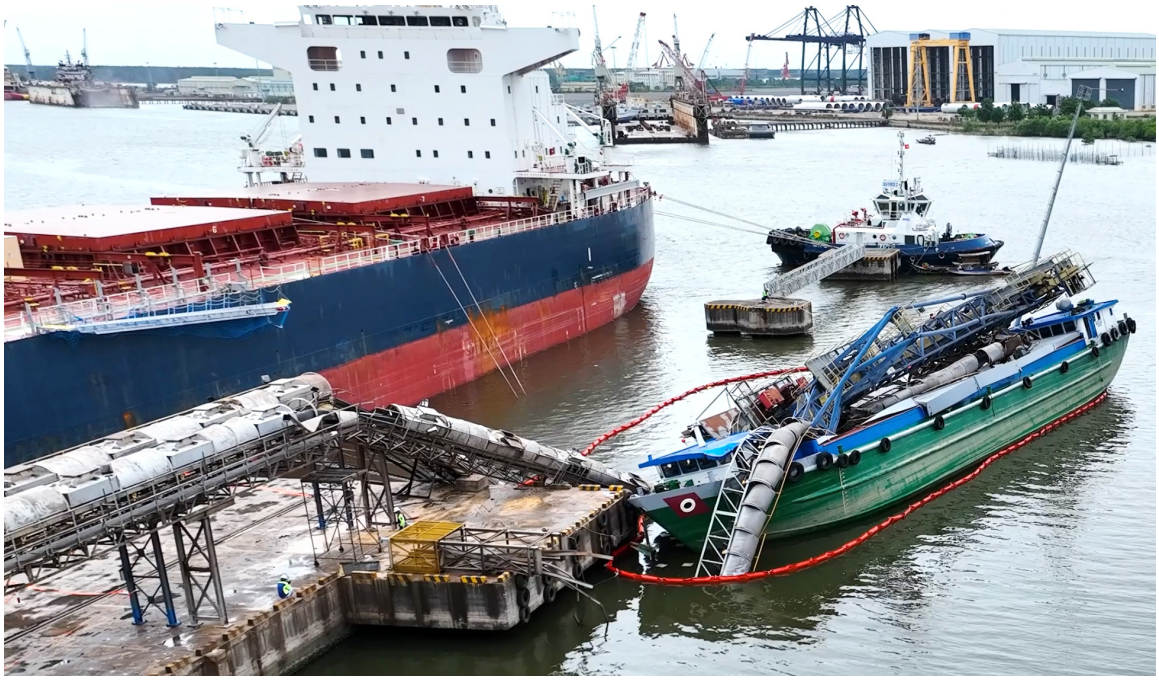

Figure 3 Port situation after the 2nd incident in July 2023.

2. MATERIALS AND METHODS

The field survey process involved four primary steps as shown in Figure 4: topographic survey, bathymetric survey, side-scan sonar, and sub-bottom profiling. This process utilizes specialized survey equipment to gather data, which is then processed through specialized software. Finally,

a unified GIS platform that offers thorough and precise mapping and analysis is built to incorporate the results.

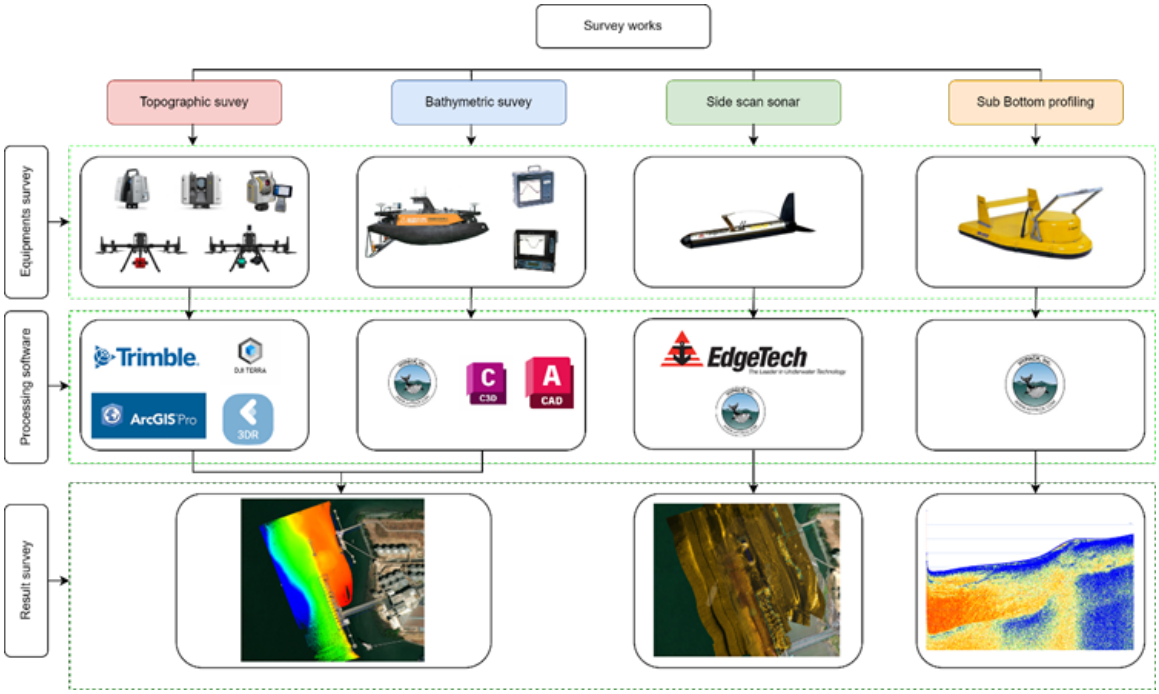

Figure 4 The process of applying advanced survey technologies.

The survey data is divided into four main groups, similar to the classification above, including: Topographic, Bathymetric, Side-scan sonar, and Sub-bottom profiling. After field surveying, the data is extracted and processed using specialized software from leading global developers in construction surveying, such as Trimble, DJI, Leica, and Hypack. Details are presented in Table 1.

Table 1 Data processing.

No.	Data	Description	Software
1	Topographic	Most of the data collected are point clouds and images	Trimble, DJI, Leica Cyclone 3DR, and ArcGIS Pro
2	Bathymetric	Most of the data collected is in x-y-z coordinate format	Autodesk AutoCAD, Autodesk Civil 3D, and Hypack
3	Side-scan sonar and Sub-bottom profiling	Collects data on the stratified layers beneath the seabed surface, including the thickness and characteristics of sediment layers	EdgeTech and Hypack

2.1 Topographic survey

Advanced techniques like 3D laser scanning and UAV aerial photography enable accurate topographic surveys. Terrestrial scanners capture high-resolution 3D point clouds for digital terrain models and construction planning. UAVs with GPS and cameras rapidly map large areas, producing orthophotos and 3D models.

3D laser scanning technology provides very precise data on the dimensions of members, especially in hard-to-reach regions (El-Omari and Moselhi 2008). Table 2 presents the most advanced laser scanning equipment currently applied to the project by major manufacturers, including Leica and Trimble.

Table 2 Specifications of 3D laser scanning devices.

Survey	Equipment	Specifications	
3D Laser scanning	Trimble SX12 	Angle measurement accuracy	1” (+ 0.3 mgon)
		Distance measurement accuracy	
		Prism mode	1.0 mm (+ 1.5 ppm)
		Direct reflex mode	2.0 mm (+ 1.5 ppm)
		Range	0.9 m to 600 m
		Range noise	1.5 mm
		Scanning accuracy (3D position accuracy)	2.5 mm
	Leica RTC 360 	Range	0.5 m to 130 m
		Range noise	0.4 mm @ 10 m, or 0.5 mm @ 20 m
		Speed	Up to 2,000,000 million points/sec
		Resolution	3.0 mm @ 10 m
UAV	Combination: Matrice 300RTK and Share 203S PRO 	Matrice 300RTK	
		Maximum speed	S-mode: 23 m/s (Sport), or P-mode: 17m/s (Positioning)
		Maximum take-off weight	9 kg
		Camera Share 203s Pro	
		Resolution	225 MP
		Image size	8192 * 5460px

UAVs are an emerging technology that can be harnessed for military, public, and civil applications (Gupta et al. 2015). Table 2 shows the drones integrated with lidar and high-resolution cameras that were used in field data collection. This step generates a 3D mesh model and point cloud model that provides both a general overview and detailed information on the project topography. Figure 5 and Figure 6 show two combinations of UAV equipment that were used for collecting comprehensive data of the study.

Figure 5 Combination: Matrice 350 RTK and SHARE UAV 203S PRO.

Figure 6 Combination: Matrice 300 RTK and Zenmuse L1 + Zenmuse P1.

Based on manufacturer guidelines and field experiments, the Zenmuse P1 excels in high-precision tasks like 3D mapping and point clouds for construction, while the Share UAV 203S Pro offers a cost-effective solution for simpler, flexible UAV projects like 3D mesh models. This dual-combo approach ensures precise data capture and efficient survey operations.

2.2 Bathymetric survey

Bathymetric surveys are crucial for coastal and offshore projects, requiring precise underwater terrain measurements. Real-Time Kinematic (RTK) technology ensures centimeter-level accuracy by providing real-time corrections through a rover and base station. As shown in Figure 7, RTK integrates with multibeam echosounder-equipped survey vessels, or USVs, delivering precise height and position data. This minimizes water level measurement errors, enhancing bathymetric accuracy (Locat and Sanfaçon 2000). Water levels are recorded every 10 minutes and calibrated using specialized software for precise depth results. However, challenges that include set-up factors, changes in water level throughout the measurement procedure, and the conversion of global coordinates to local coordinates may affect the results of the RTK method (Gillins et al. 2022). The RTK technique can be summarized as in Figure 8.

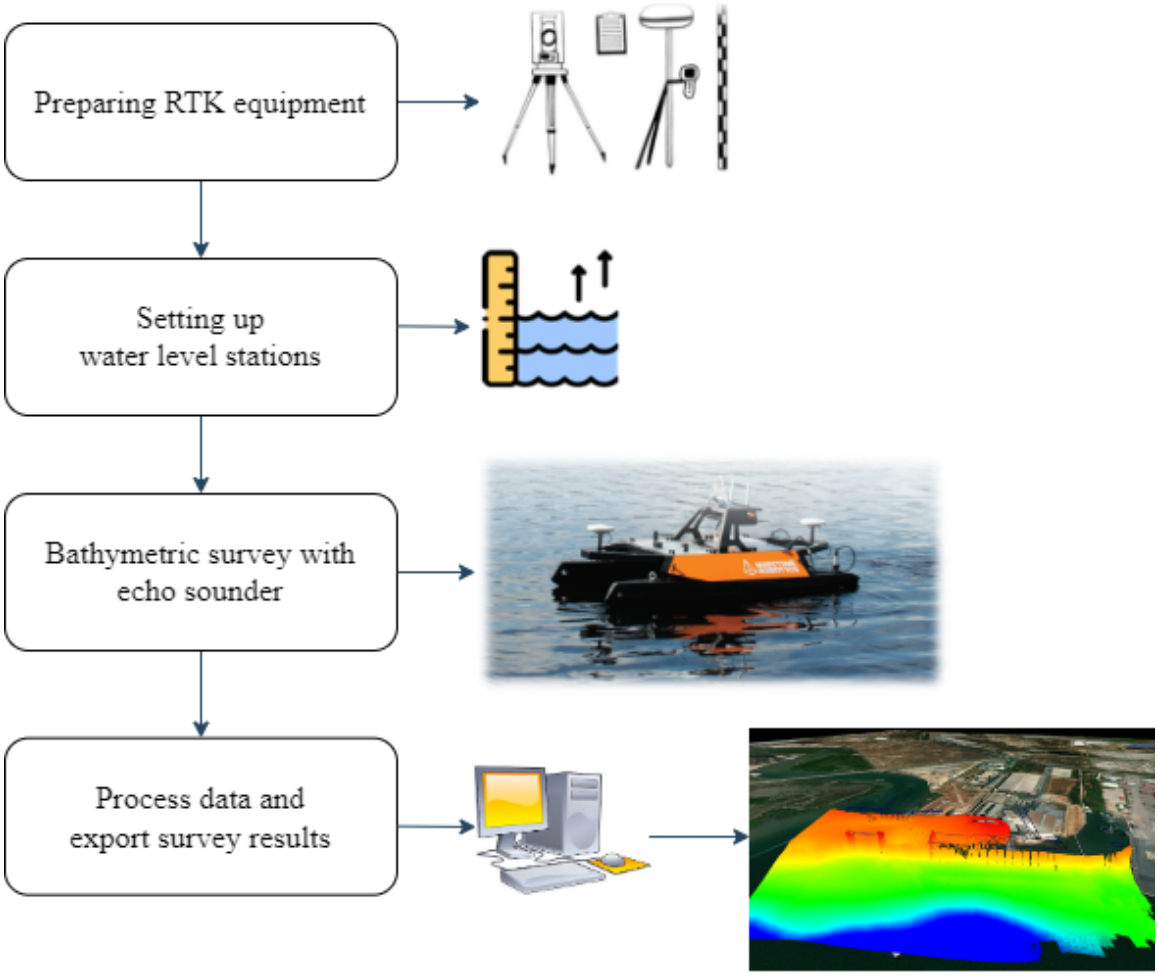

Figure 7 Bathymetric survey using Real Time Kinematic (RTK) technique.

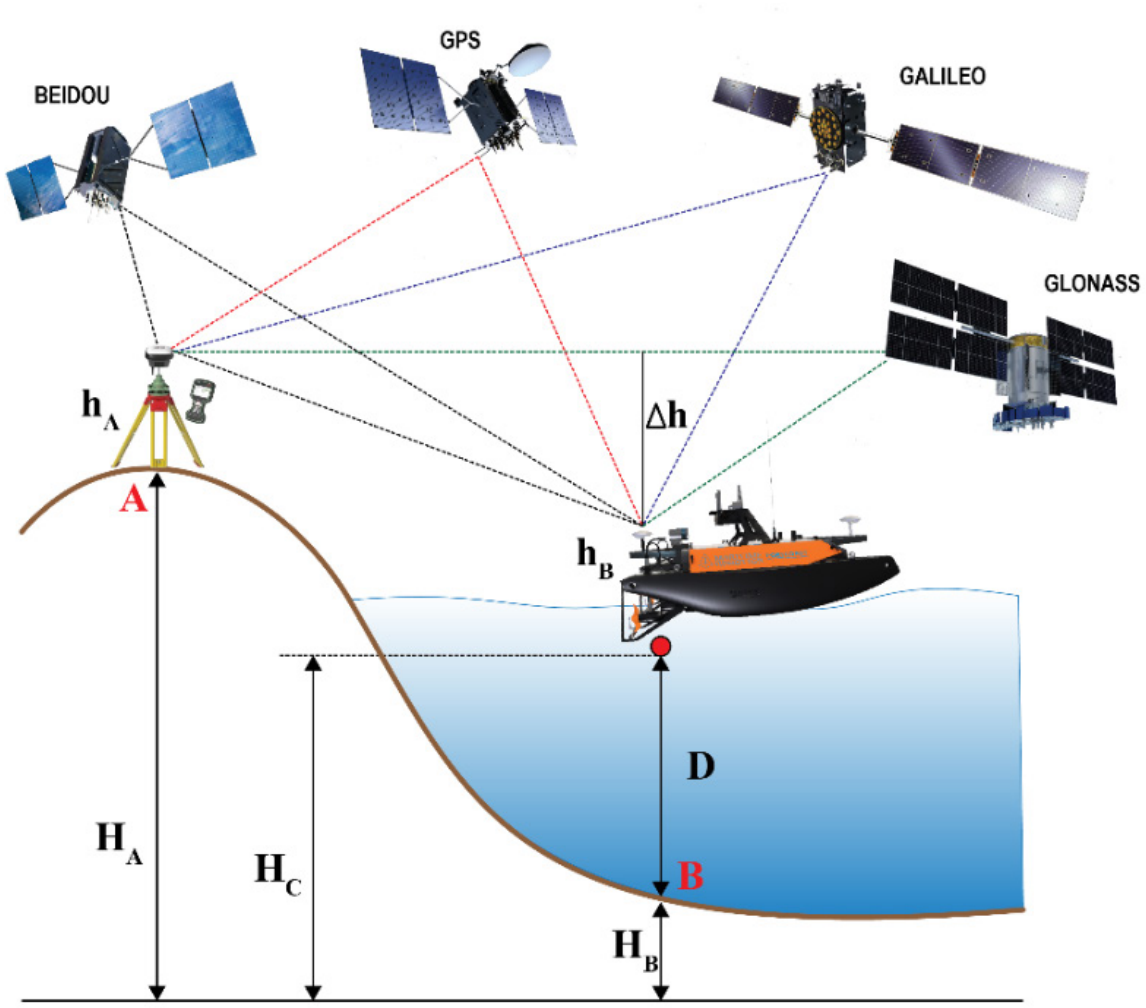

Figure 8 RTK (Real Time Kinematic) measurement technique.

The diagram above describes the principle of determining the bottom height by RTK technique, in which:

- Δh is the high difference between the phase center of the base station antenna and the dynamic station, determined by the RTK technique.
- H_A is the height of the landmark relative to the reference ellipsoid face.
- H_c is the height of the bottom of the reverberator sensor head compared to the reference ellipsoid side.
- h_A is the antenna height of the base station relative to the landmark, measured in rulers with an accuracy of about 5 mm.
- h_B is the height calculated from the antenna phase center of the dynamic station to the bottom of the echo sensor head at the location of the survey vessel.
- D is the depth calculated from the bottom of the reverberator sensor to the bottom surface, measured by a reverberation depth meter.

- H_B is the elevation of the river bottom relative to the reference ellipsoid surface, calculated according to the formula.
- $H_B = H_C - D$
- H_C is the height of the bottom of the reverberator sensor head.
- $H_C = h_A + H_A - \Delta h - h_B$

The RTK technique delivers precise ground position and antenna altitude during measurement, eliminating errors in water level-based depth determination and ensuring maximum accuracy in hydrographic surveys.

2.3 Marine obstacles detection by side-scan sonar

Side-scan sonar is widely used in ocean engineering for high-resolution seabed imaging and detecting underwater targets (Healy et al. 2015). In this study, the vessel collision caused multiple wharf structures to collapse and sink into the riverbed, necessitating obstacle scanning to identify obstructions for future operations. Using a digital logger to continuously collect data, side-scan sonar excels in high-precision obstacle detection, especially when paired with an echo sounder (Figure 9). The data are obtained in a digitized form that allows the oblique correction number to be calculated to produce a relatively flat image (Manik 2011).

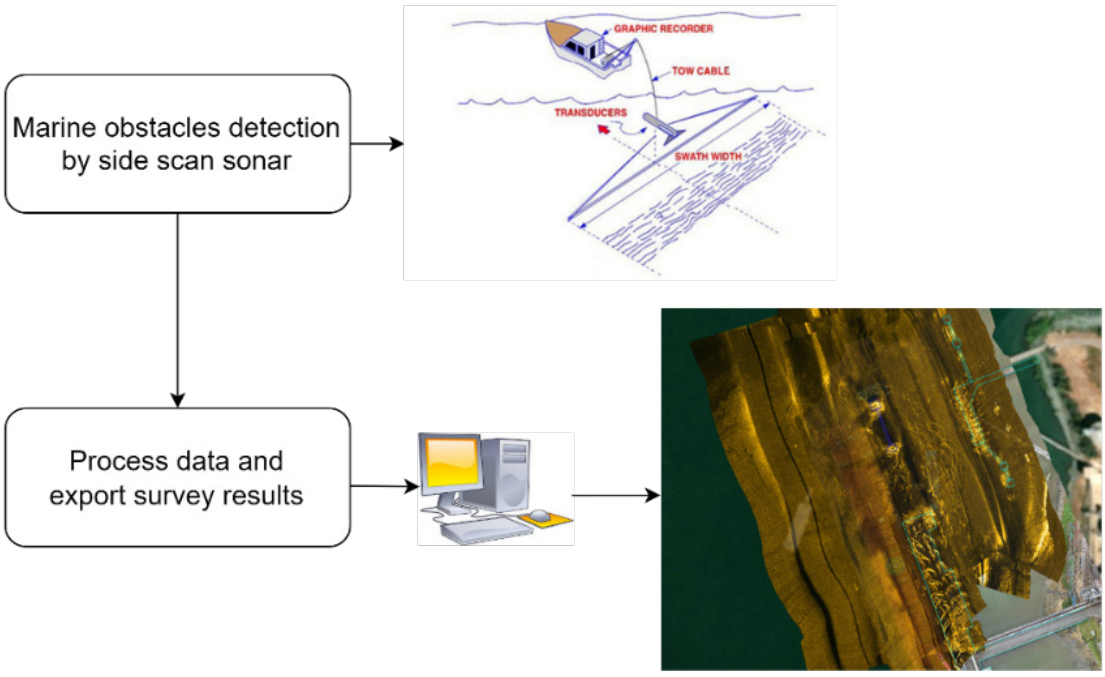

Figure 9 Marine obstacles detection by side-scan sonar process.

Post-accident assessment revealed severe damage to several berth piles (Figure 10 and Figure 11), reducing the port's operational capacity. Obstacle clearance removed debris hindering

navigation and repairs, causing minor seabed scratches and dents that did not impact repair plans. The wharf was deemed structurally sound and ready for restoration.

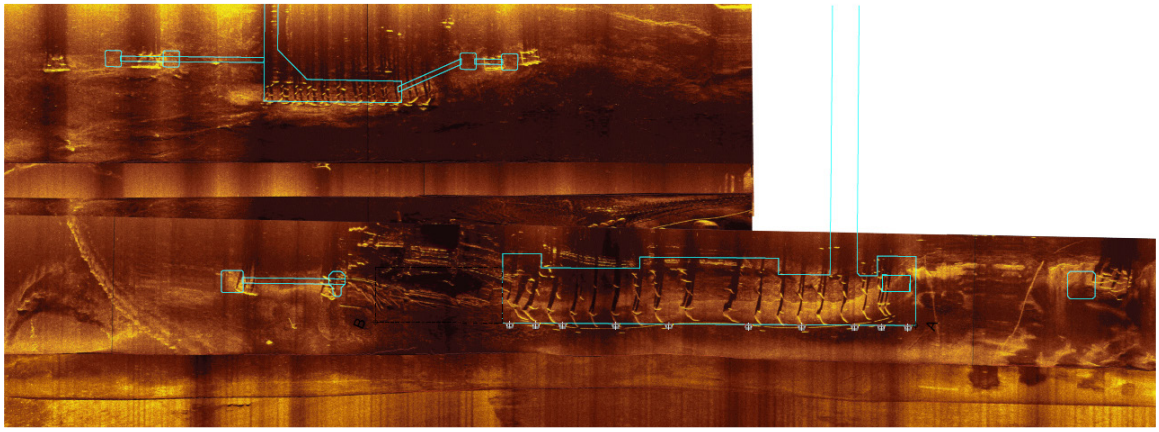

Figure 10 Post-accident condition of the wharf.

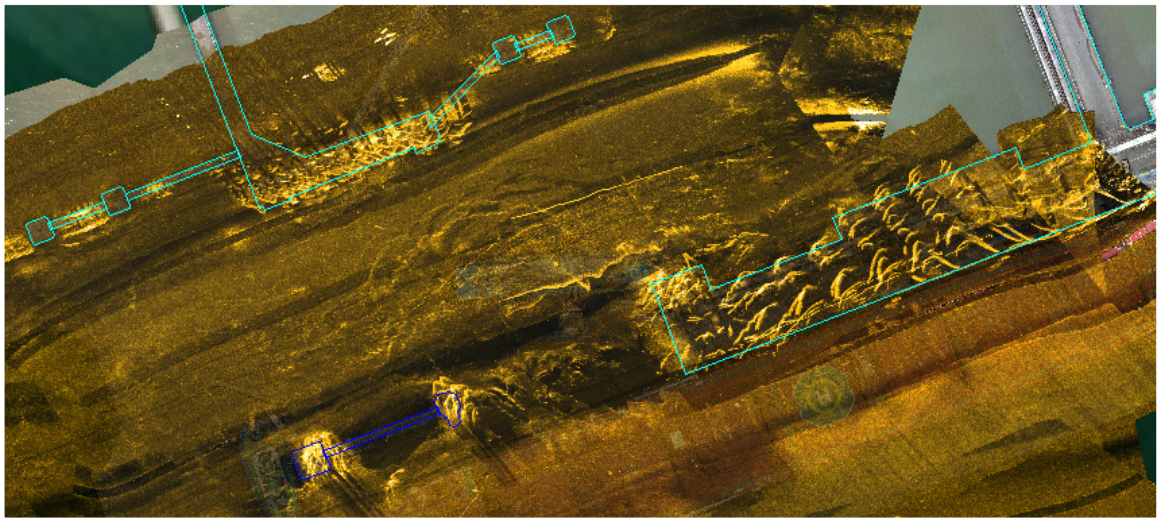

Figure 11 Wharf structure condition after obstacle clearance.

2.4 Sub-bottom profiling

In marine and underwater surveys, sub-bottom profiling is an invaluable tool for investigating and determining the layers of rock and silt beneath the riverbed or seabed. It works by releasing low-frequency sound waves into the seawater, which are reflected by the various layers below. An image of the subsurface layers is produced by capturing and processing these reflected signals (Figure 12). A sub-bottom profiler is a type of sonar system—a geophysical survey tool that uses sound to map beneath the seafloor (NOAA Ocean Exploration 2023; NOAA Ocean Exploration 2014; Saleh and Rabah 2016).

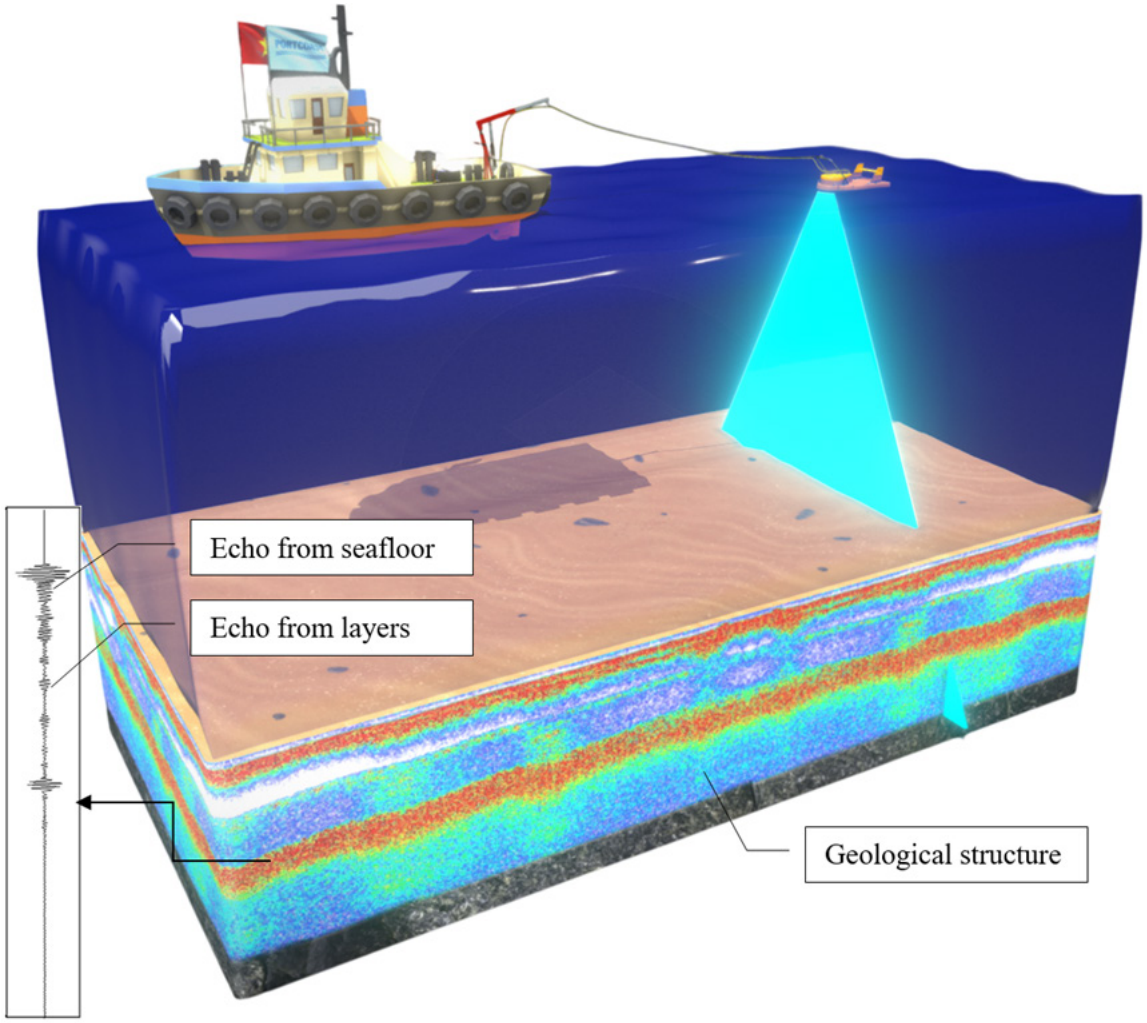

Figure 12 Schematic representation of a survey vessel undertaking sub-bottom profiling.

3. RESULTS AND DISCUSSION

To comprehensively assess the post-incident conditions, four survey techniques were employed: topographic, bathymetric, side-scan sonar, and sub-bottom profiling. The resulting dataset supported essential tasks such as obstacle clearance, damage assessment, repair design, and reconstruction.

To ensure the accuracy of the generated 3D point cloud and 3D mesh models, ground control points (GCPs) were strategically placed across the survey area. The precise (X, Y, Z) coordinates of each GCP were measured using electronic total station equipment. By identifying corresponding points on the 3D models and calculating the coordinate differences (X, Y, Z), the root mean square error (RMSE) was determined using Equation 1 (Gillins et al. 2022):

$$RMSE = \sqrt{\frac{\Sigma_{i=1}^{n}[x_i - f(x_i)^2]}{n}} \quad (1)$$

In this formula, x_i represents the coordinates from the check survey for the *n* sample points, while $f(x_i)$ denotes the coordinates obtained from the map or from a project utilizing LiDAR, laser scanning, or 3D photogrammetry.

The results, summarized in Table 3, indicate an RMSE of 0.021 m for the X-axis, 0.021 m for the Y-axis, and 0.019 m for the Z-axis, demonstrating the accuracy of the 3D photogrammetry technology. While this level of precision is suitable for many applications, it falls short of the higher accuracy achieved by 3D laser scanning and LiDAR-UAV technologies, especially along the Y and Z axes. Therefore, 3D photogrammetry is best suited for applications requiring medium accuracy rather than high precision for capturing fine details.

Table 3 Detailed comparison of point position errors between GCPs and 3D mesh model.

Point ID	3D Photogrammetry model			GCPs			Deviation		
	x	y	z	x	y	z	ΔX	ΔY	ΔZ
P1	420795.526	1166248.837	3.150	420795.535	1166248.848	3.159	-0.009	-0.011	-0.009
P2	420802.346	1166195.060	3.188	420802.338	1166195.051	3.195	0.008	0.009	-0.007
P3	420819.817	1166199.063	3.139	420819.828	1166199.075	3.148	-0.011	-0.012	-0.009
P4	420834.778	1166114.748	3.160	420834.787	1166114.737	3.151	-0.009	0.011	0.009
P5	420847.362	1166122.133	3.139	420847.373	1166122.144	3.130	-0.011	-0.011	0.009
P6	420881.794	1166043.699	3.173	420881.785	1166043.688	3.161	0.009	0.011	0.012
P7	420872.279	1166013.482	3.169	420872.268	1166013.492	3.158	0.011	-0.010	0.011
P8	420895.199	1166021.734	3.118	420895.208	1166021.725	3.111	-0.009	0.009	0.007
P9	420907.295	1165963.445	3.097	420907.288	1165963.455	3.107	0.007	-0.010	-0.010
P10	420969.104	1166078.759	3.153	420969.115	1166078.748	3.143	-0.011	0.011	0.010
						RMSE (m)	0.021	0.021	0.019

In contrast, 3D Laser Scanning technology exhibited exceptional accuracy, with minimal RMSE values of 0.012 m, 0.008 m, and 0.007 m for the X, Y, and Z axes, respectively (Table 4). This high precision makes 3D Laser Scanning an ideal choice for applications requiring detailed spatial data, such as those involving complex structures or intricate details.

Table 4 Detailed comparison of point position errors between GCPs and 3D point cloud data from laser scanning.

Point ID	3D Point Cloud			GCPs			Deviation		
	x	y	z	x	y	z	ΔX	ΔY	ΔZ
TLS-1	420795.540	1166248.844	3.162	420795.535	1166248.848	3.159	0.005	-0.004	0.003
TLS-2	420802.334	1166195.057	3.196	420802.338	1166195.051	3.195	-0.004	0.006	0.001
TLS-3	420819.836	1166199.073	3.151	420819.828	1166199.075	3.148	0.008	-0.002	0.003
TLS-4	420834.780	1166114.733	3.155	420834.787	1166114.737	3.151	-0.007	-0.004	0.004
TLS-5	420847.369	1166122.142	3.132	420847.373	1166122.144	3.130	-0.004	-0.002	0.002
TLS-6	420881.778	1166043.691	3.165	420881.785	1166043.688	3.161	-0.007	0.003	0.004
TLS-7	420872.262	1166013.496	3.155	420872.268	1166013.492	3.158	-0.006	0.004	-0.003
TLS-8	420895.205	1166021.722	3.108	420895.208	1166021.725	3.111	-0.003	-0.003	-0.003
TLS-9	420907.291	1165963.450	3.103	420907.288	1165963.455	3.107	0.003	-0.005	-0.004
TLS-10	420969.111	1166078.751	3.147	420969.115	1166078.748	3.143	-0.004	0.003	0.004
						RMSE (m)	0.012	0.008	0.007

LiDAR-UAV technology exhibited consistent and moderate accuracy across all axes, with an RMSE of 0.015 m for the X-axis, 0.015 m for the Y-axis, and 0.012 m for the Z-axis. This makes LiDAR-UAV well-suited for collecting data over large, inaccessible areas, offering a balance between accuracy and efficiency. While not as precise as 3D Laser Scanning, LiDAR-UAV provides a reliable solution for various applications, as shown in Table 5 (Wang and Kim 2019).

Table 5 Detailed comparison of point position errors between GCPs and 3D point cloud data from LiDAR mounted on a UAV.

Point ID	3D Point Cloud			GCPs			Deviation		
	x	y	z	x	y	z	ΔX	ΔY	ΔZ
L1	420795.528	1166248.841	3.153	420795.535	1166248.848	3.159	-0.007	-0.007	-0.006
L2	420802.345	1166195.044	3.191	420802.338	1166195.051	3.195	0.007	-0.007	-0.004
L3	420819.820	1166199.068	3.144	420819.828	1166199.075	3.148	-0.008	-0.007	-0.004
L4	420834.780	1166114.743	3.158	420834.787	1166114.737	3.151	-0.007	0.006	0.007
L5	420847.380	1166122.136	3.134	420847.373	1166122.144	3.130	0.007	-0.008	0.004
L6	420881.778	1166043.681	3.157	420881.785	1166043.688	3.161	-0.007	-0.007	-0.004
L7	420872.274	1166013.500	3.166	420872.268	1166013.492	3.158	0.006	0.008	0.008
L8	420895.215	1166021.731	3.116	420895.208	1166021.725	3.111	0.007	0.006	0.005
L9	420907.293	1165963.461	3.102	420907.288	1165963.455	3.107	0.005	0.006	-0.005
L10	420969.109	1166078.742	3.148	420969.115	1166078.748	3.143	-0.006	-0.006	0.005
						RMSE (m)	0.015	0.015	0.012

For bathymetric data, comparisons between multibeam and single-beam measurements were conducted. Both single-beam and multi-beam depth measurement methods were employed to maximize data reliability. The accuracy of multi-beam echo sounding is influenced by factors such as operating frequency, beam scanning angle, system stability, and sensor accuracy. To maintain accuracy, the middle beam of the multi-beam system was regularly checked against

single-beam measurements. The acceptable error limit for these measurements depends on the equipment specifications and the required map scale.

The survey results identified potential conflicts between submerged piles and proposed repair work, streamlining the design process. Figure 13 illustrates a 3D point cloud model suitable for BIM integration, while Figure 14 presents bathymetric data with depths ranging from -25.9 m to -1.0 m. The combined survey data resulted in a detailed 3D model integrated into a GIS platform, along with a color-coded bathymetric map. This comprehensive analysis underscores the necessity of clearing underwater obstructions to restore the wharf to full operational capacity.

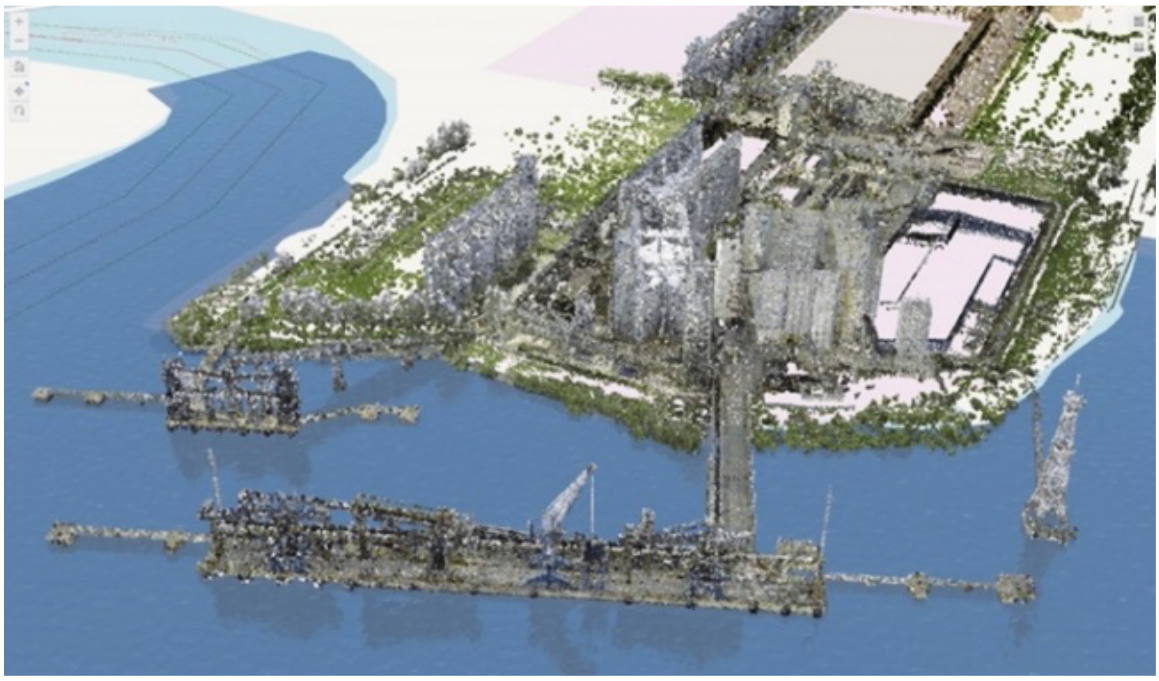

Figure 13 3D point cloud model of Interflour port.

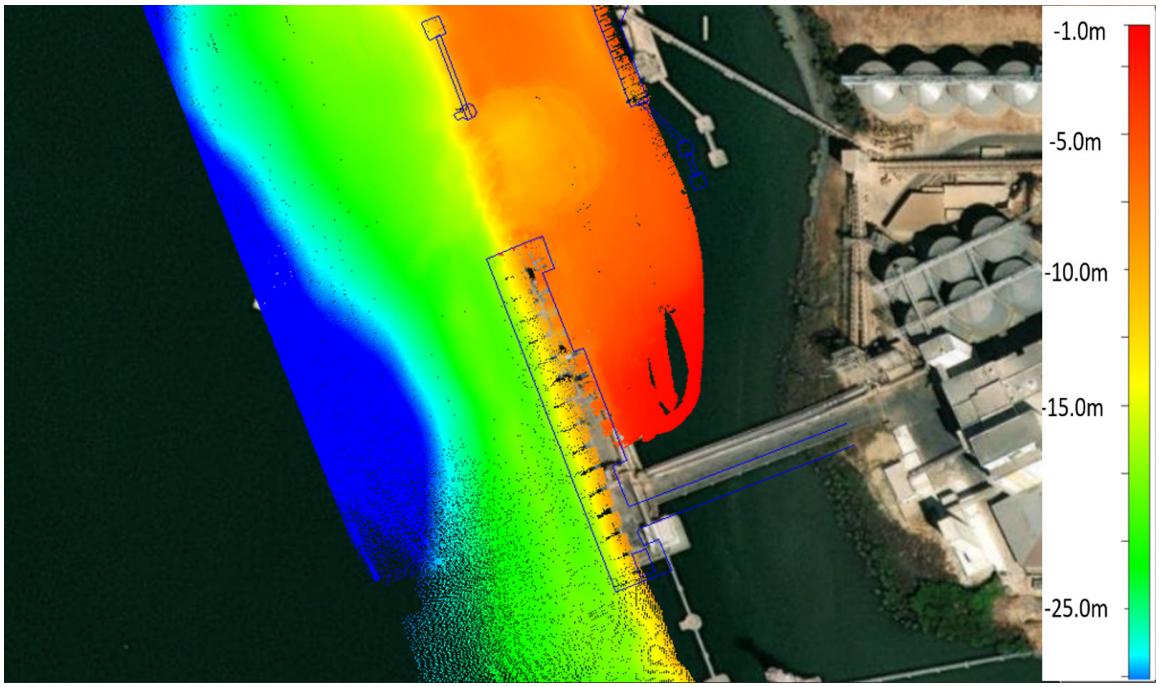

Figure 14 Bathymetric map in the waterfront area.

Modern technologies significantly enhance survey accuracy, especially in post-accident scenarios involving broken piles, submerged structures, and collapsed facilities. Precise obstacle localization is crucial to prevent repair conflicts, such as inadvertently driving new piles into debris. Figure 15 demonstrates the use of side-scan sonar to detect seabed obstacles, while Figure 16 illustrates sub-bottom profiling to reveal underlying geological layers.

Following the vessel collision, debris sank into the silt-covered seabed, making it undetectable by standard echo sounding techniques. However, side-scan sonar and sub-bottom profiling proved effective in identifying and locating these obstacles, enabling their clearance.

The side-scan sonar provides a detailed image of the seabed, accurately mapping the bottom surface of obstacles and conducting precise depth measurements of suspected areas. While the sub-bottom profiling results are primarily qualitative, they can be correlated with nearby geological borehole data to make more definitive stratigraphic conclusions. In this specific case, the survey results clearly indicate the need to remove damaged piles from the riverbed before initiating repair work. Furthermore, the clear and uniform nature of the soil layers in this area mitigates the need for additional verification through nearby boreholes.

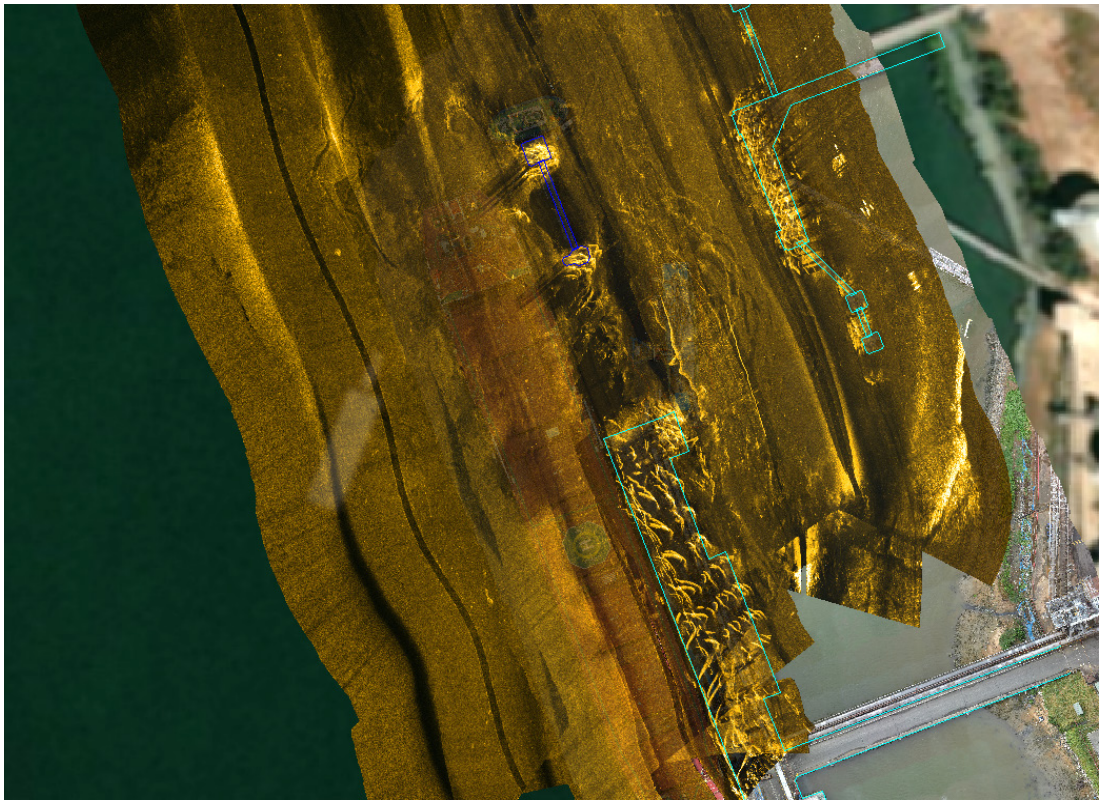

Figure 15 Seabed survey result using side-scan sonar.

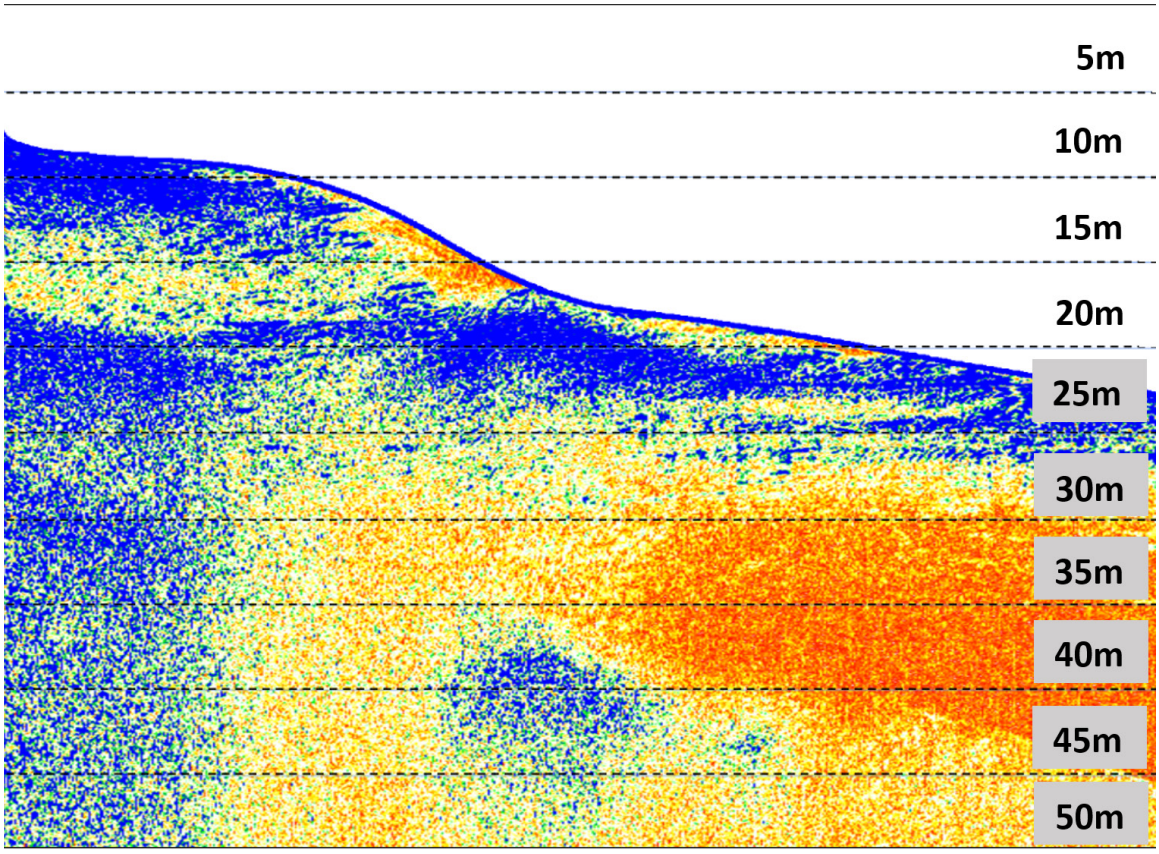

Figure 16 Seabed sub-bottom profiling.

By combining side-scan sonar and sub-bottom profiling, design engineers gained a comprehensive understanding of the post-incident underwater landscape. This knowledge allowed them to minimize design conflicts and ensure the future structure's bearing capacity. Careful processing of the survey data yielded a highly detailed, precise point cloud model. This model seamlessly integrated with a GIS platform, enabling efficient project information management.

Furthermore, by leveraging comprehensive data from bathymetric surveys, obstacle detection, and sub-bottom profiling, BIM models were created and integrated with the GIS model. This powerful combination provided an accurate representation of existing structures and objects, facilitating thorough visualization and evaluation of potential modifications.

In conclusion, bathymetric surveying, obstacle detection, and sub-bottom profiling are essential prerequisites for successful BIM implementation in infrastructure projects. This integrated approach significantly reduces conflicts, errors, and problems throughout the project lifecycle, from design to construction and operation.

4. CONCLUSION

This research innovatively combined four survey techniques (topographic, bathymetric, sub-bottom profiling, and maritime obstacle detection) within a single project. The resulting data was seamlessly integrated into a user-friendly GIS platform, providing engineers with a

comprehensive view of all construction survey information. This integration of scientific advancements and technological tools enables high-precision data collection and clear visual representation, which is particularly crucial for projects with a history of collisions or incidents. Furthermore, the use of modern equipment enhances both the accuracy and flexibility of data acquisition, especially in challenging and hard-to-reach locations. These advancements significantly improve the accuracy, flexibility, and efficiency of data collection and representation in existing condition surveys, highlighting the importance of adapting scientific and technological advancements to surveying methodologies.

ACKNOWLEDGMENTS

The authors sincerely thank to Portcoast Consultant Corporation, Vietnam (Portcoast), for providing the essential resources required to conduct this study. We also express our acknowledgements to the Ho Chi Minh City University of Technology (HCMUT, VNU-HCM) for their support and assistance.

REFERENCES

Ehlers, S. 2011. "A review of collision and grounding damage assessment methods." *Marine Systems and Ocean Technology* 6: 5–15. https://doi.org/10.1007/BF03449252

El-Omari, S., and O. Moselhi. 2008. "Integrating 3D Laser Scanning and Photogrammetry for Progress Measurement of Construction Work". *Automation in Construction* 18 (1): 1–9. https://doi.org/10.1016/j.autcon.2008.05.006

Gillins, D.T., M.L. Dennis, and A.Y. Ng. 2022. *Surveying and Geomatics Engineering: Principles, Technologies, and Applications.* American Society of Civil Engineers, Virginia, USA, pp 550. https://doi.org/10.1061/9780784416037

Gupta, L., R. Jain, and G. Vaszkun. 2015. "Survey of Important Issues in UAV Communication Networks." *IEEE Communications Surveys and Tutorials* 18 (2): 1123–1152. https://doi.org/10.1109/COMST.2015.2495297

Healy C.A., J.J. Schultz, K. Parker, and B. Lowers. 2015. "Detecting Submerged Bodies: Controlled Research Using Side-scan Sonar to Detect Submerged Proxy Cadavers." *Journal of Forensic Sciences* 60 (3): 743–752. https://doi.org/10.1111/1556-4029.12671

Khoi, T.P.M., L.D. Khoa, N.H.A Thu, and N.D. Thao. 2024. "Application of BIM-GIS in Assessing and Re-designing of Wharf Structure after Vessel Collision". *The 35th PIANC World Congress 2024*, April–May 2024, Cape Town, South Africa, pp. 425–431.

Locat, J., and R. Sanfaçon. 2000. "Multibeam surveys: a major tool for geosciences." In *Proceedings of the Canadian Hydraugraphics Conference*, Montréal, pp. 1–11.

Manik, H.M. 2011. *Underwater Acoustic Detection and Signal Processing Near the Seabed, in Sonar Systems.* Edited by Nikolai Kolev (First Edition). InTech, Croatia. pp. 255–274. https://doi.org/10.5772/17499

NOAA Ocean Exploration. 2014. Sub-bottom Profiling. Accessed on May 5, 2024. https://oceanexplorer.noaa.gov/okeanos/explorations/ex1404/logs/sept24/sept24.html.

NOAA Ocean Exploration. 2023. Sub-bottom Profiler. Accessed on May 5, 2024. https://oceanexplorer.noaa.gov/technology/sub-bottom-profiler/sub-bottom-profiler.html.

Saleh, M., and M. Rabah. 2016. “Seabed Sub-bottom Sediment Classification using Parametric Sub-bottom Profiler”. *NRIAG Journal of Astronomy and Geophysics* 5 (1): 87–95. https://doi.org/10.1016/j.nrjag.2016.01.004

Thao, N.D., T.P.M. Khoi, L.T. Anh, and L.B. Binh. 2024. “BIM-GIS Integration for Port Planning: Case Study of Hai Phong Port Cluster in Vietnam.” *The 35th PIANC World Congress 2024*, April–May 2024, Cape Town, South Affrica, pp. 432–437.

Wang, Q., and M.-K. Kim. 2019. “Applications of 3D point cloud data in the construction industry: A fifteen-year review from 2004 to 2018.” *Advanced Engineering Informatics* 39, 306–319. https://doi.org/10.1016/j.aei.2019.02.007